AGU PUBLICATIONS

Journal of Geophysical Research – Solid Earth

Supporting Information for

Vertically extensive magma reservoir revealed from joint inversion and quantitative interpretation of seismic and gravity data

Michele Paulatto[1], Max Moorkamp[2], Stefanie Hautmann[3], Emilie Hooft[4], Joanna V. Morgan[1], R. Stephen J. Sparks[5]

[1] Department of Earth Science and Engineering, Imperial College London, London, UK

[2] Department of Earth and Environmental Sciences, Ludwig Maximilian University of Munich, Munich, Germany

[3] Department of Earth Sciences, ETH Zurich, Zurich, Switzerland

[4] Department of Earth Sciences, University of Oregon, Eugene (OR), USA

[5] School of Earth Sciences, University of Bristol, Bristol, UK

Contents of this file

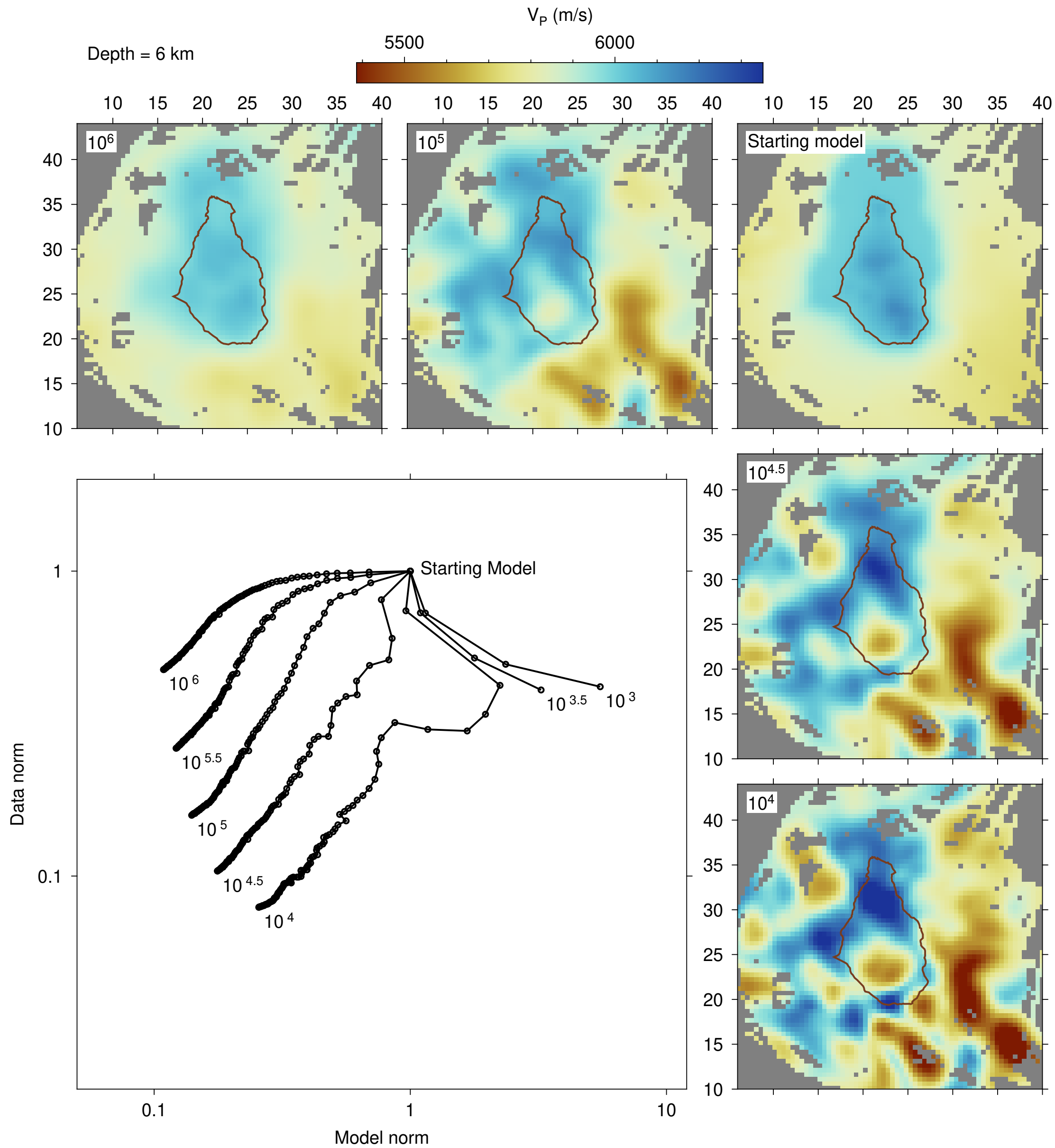

Figure S1. Trade-off curve (L-curve) for standalone seismic inversion showing the effect of changing the strength of the seismic velocity model regularization weight $\boldsymbol{\lambda_s}$ between 10^3 and 10^6. The inversions with $\boldsymbol{\lambda_s = 10^3}$ and $\boldsymbol{\lambda_s = 10^{3.5}}$ became trapped inside a local minimum and were halted. The panels on the top and right show cross-sections at 6 km depth through the starting model and the final models after 100 iterations.

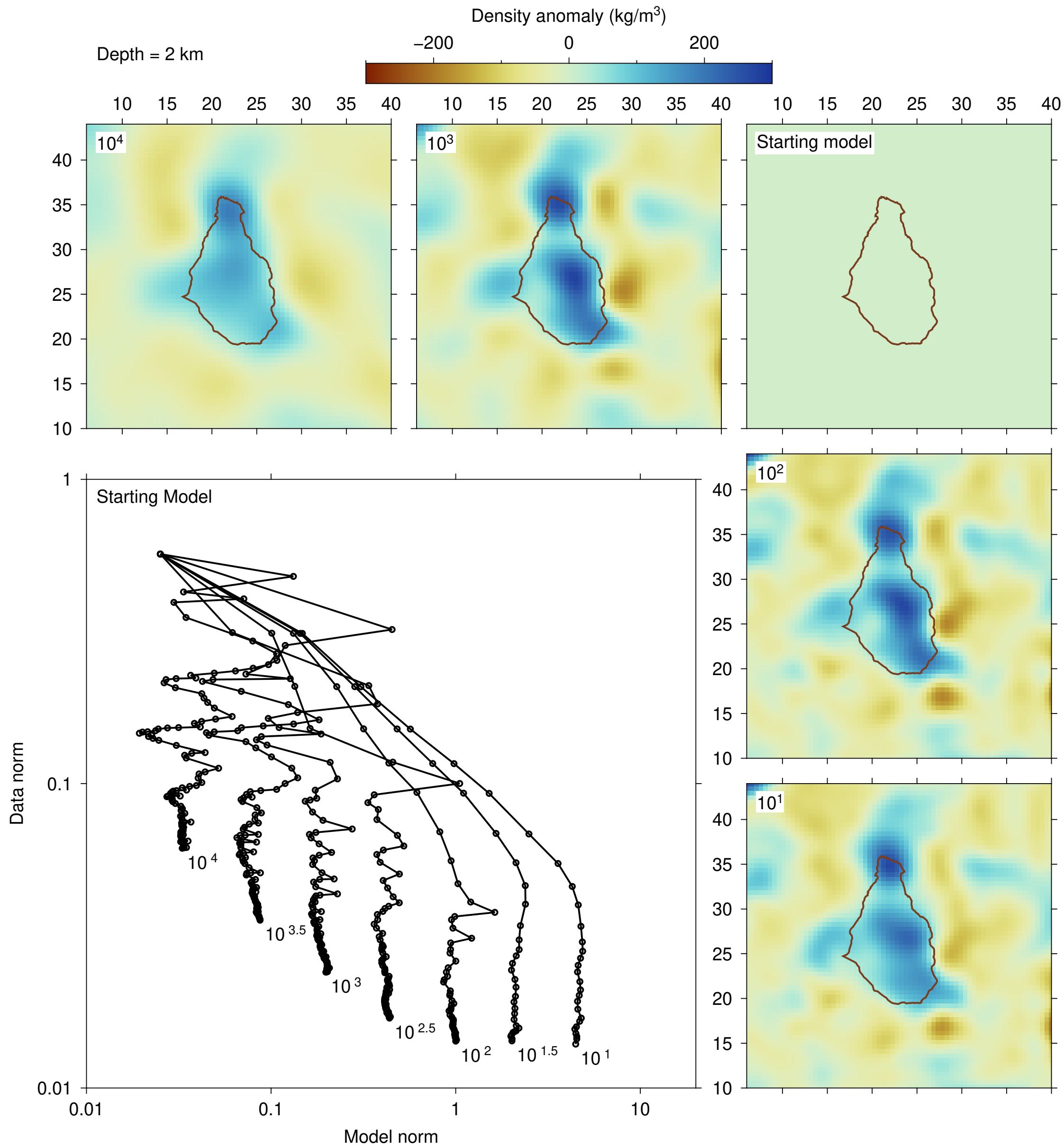

Figure S2. Trade-off curve (L-curve) for standalone gravity inversion showing the effect of changing the strength of the density model regularization weight λ_ρ between 10^1 and 10^4. The panels on the top and right show cross-sections at 2 km depth through the starting model and the final models after 100 iterations.

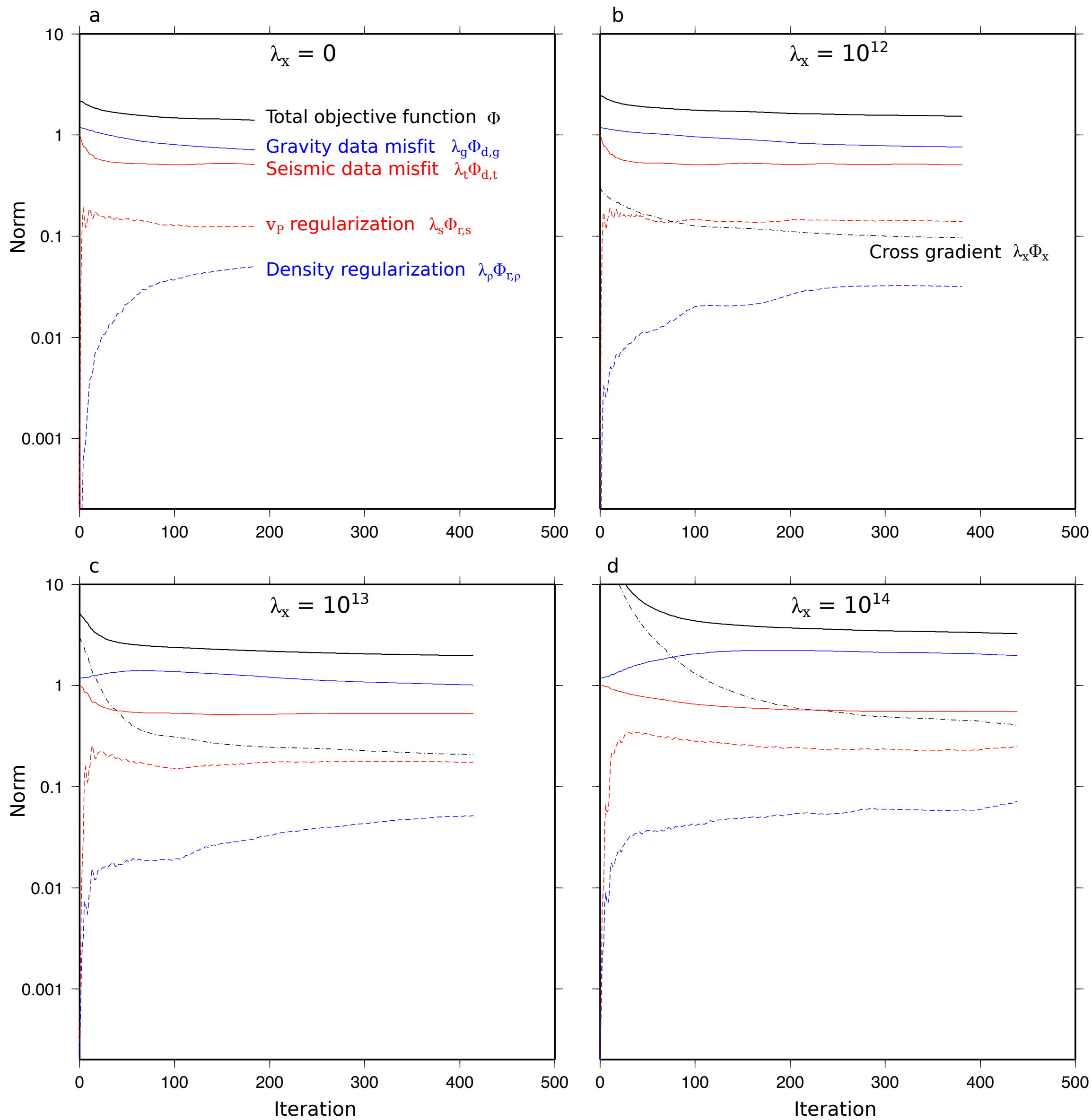

Figure S3. Evolution of the different terms of the objective function during joint inversion of seismic traveltimes and gravity data. Each term is normalized with respect to the starting seismic data misfit $\boldsymbol{\lambda_t \Phi_{d,t}(i = 0)}$. Panels a to d correspond to increasing values of the cross-gradient weight $\boldsymbol{\lambda_x}$. Notice how increasing the cross-gradient weight slows down the convergence rate. The optimal $\boldsymbol{\lambda_x}$ is in the range $10^{12} – 10^{13}$, as it gives a cross-gradient term of the same order of magnitude as the seismic velocity and density regularization terms and doesn't significantly degrade the final data misfit.

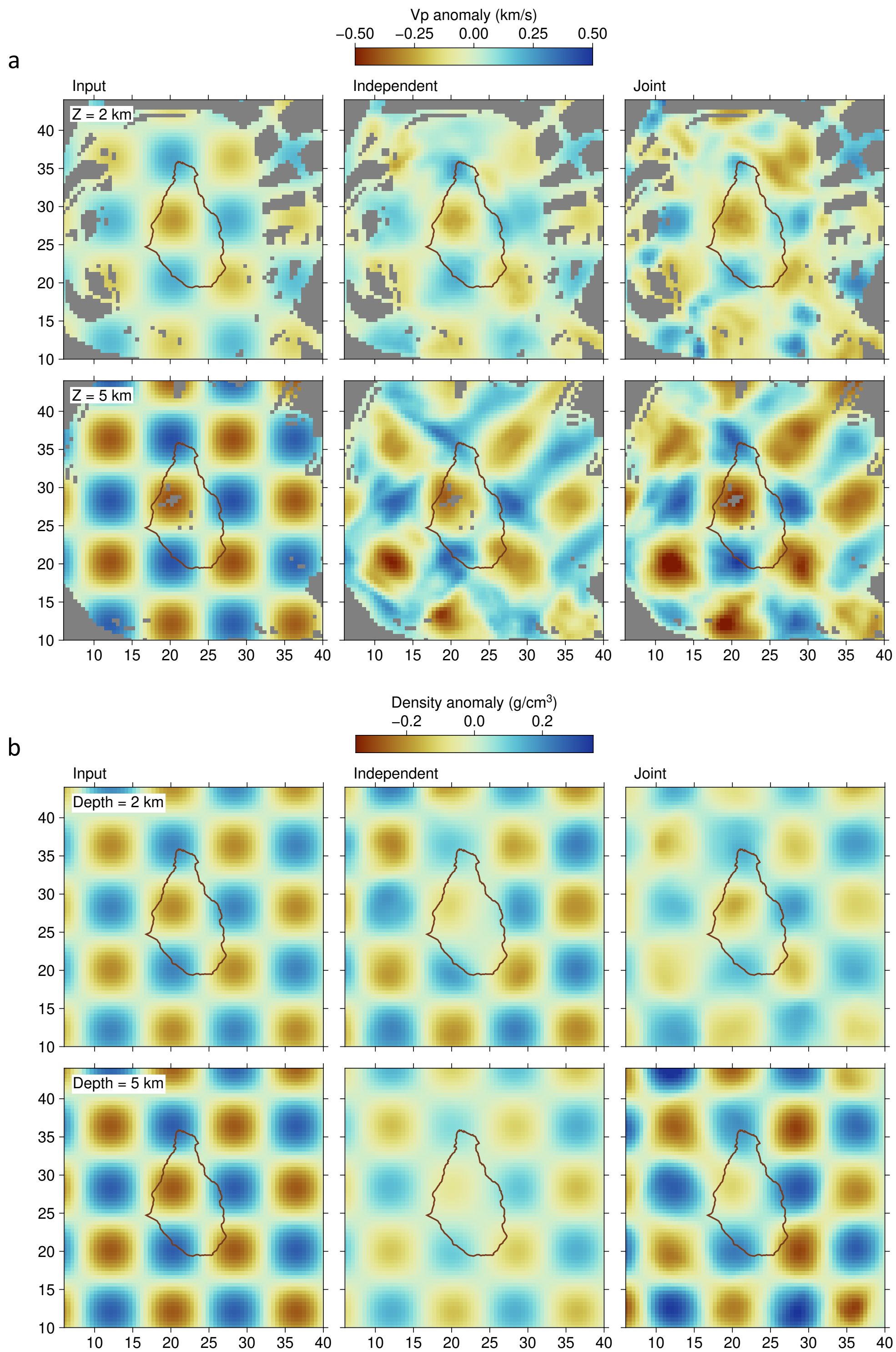

Figure S4. Comparison of checkerboard recovery for independent and joint inversions. (a) v_P checkerboard. (b) density checkerboard. Anomaly size = 8x8x8 km. Single checkerboard layer centered at 5 km depth.

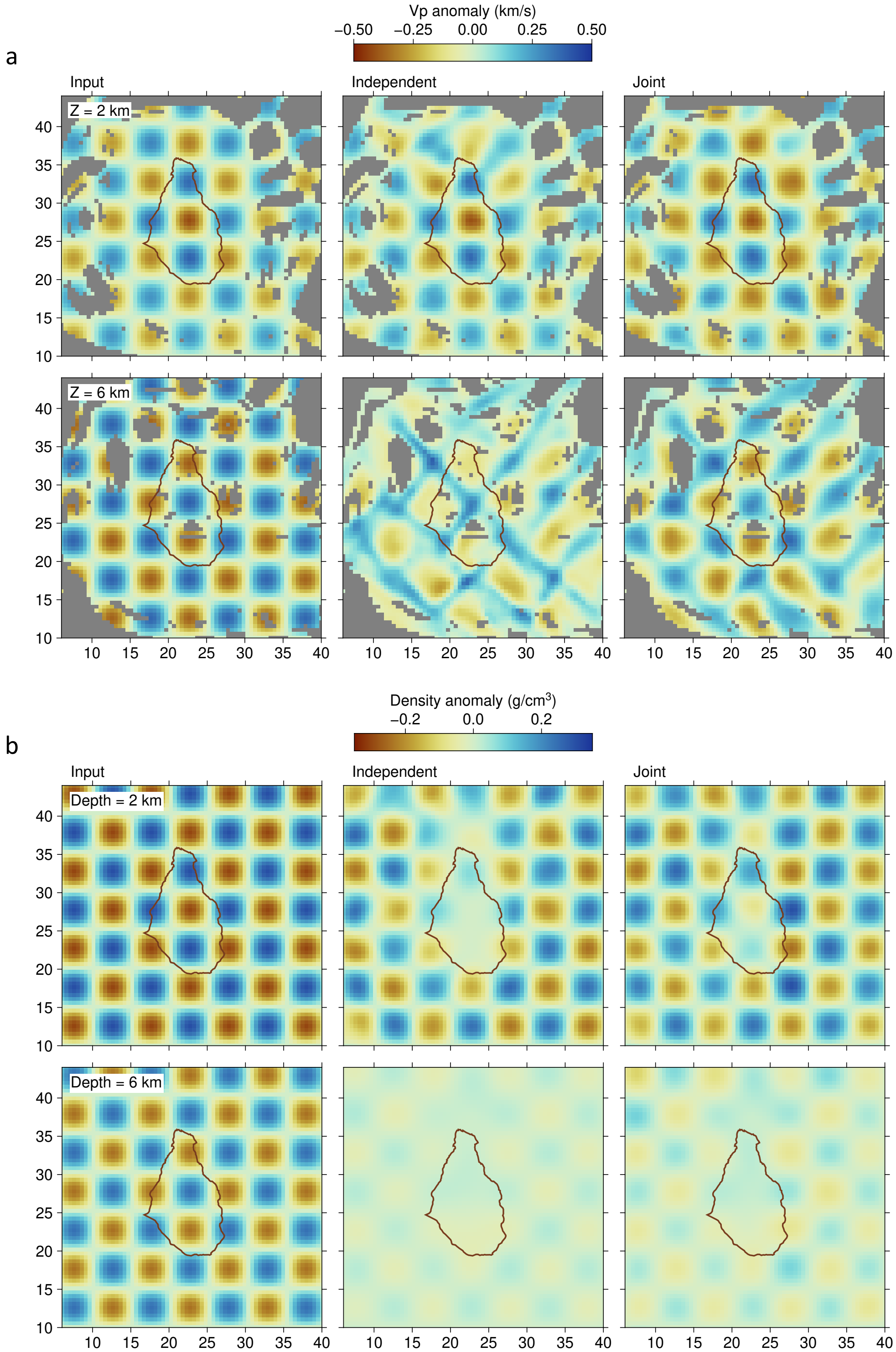

Figure S4. Comparison of checkerboard recovery for independent and joint inversions. (a) v_P checkerboard. (b) density checkerboard. Anomaly size = 5x5x5 km. Double checkerboard layers centred at 2 and 7 km depth.

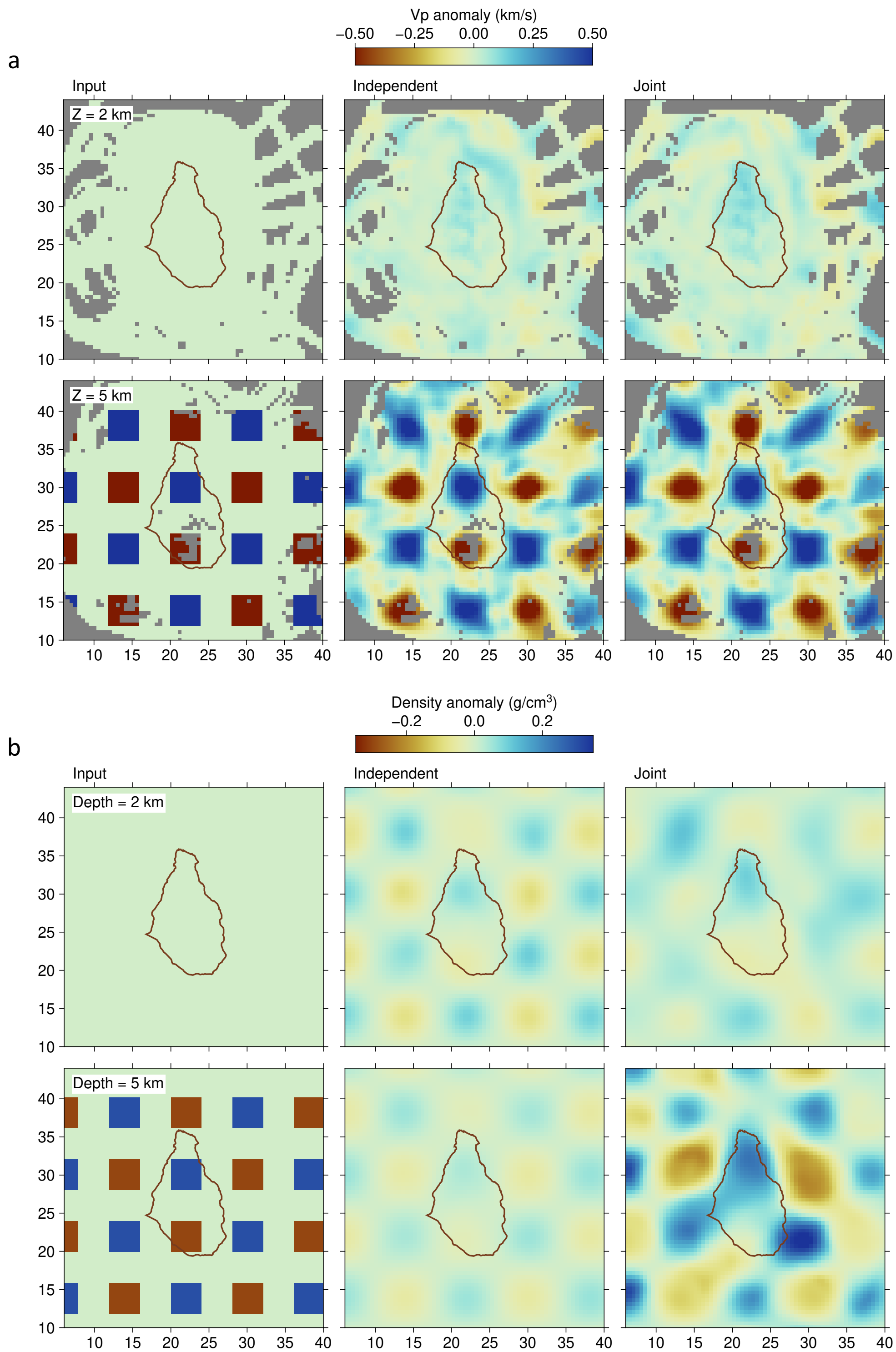

Figure S4. Comparison of boxcar pattern recovery for independent and joint inversions. (a) $\boldsymbol{v_P}$ boxcar test. (b) density boxcar test. Anomaly size = 5x5x5 km. Single boxcar layer centered at 5 km depth.

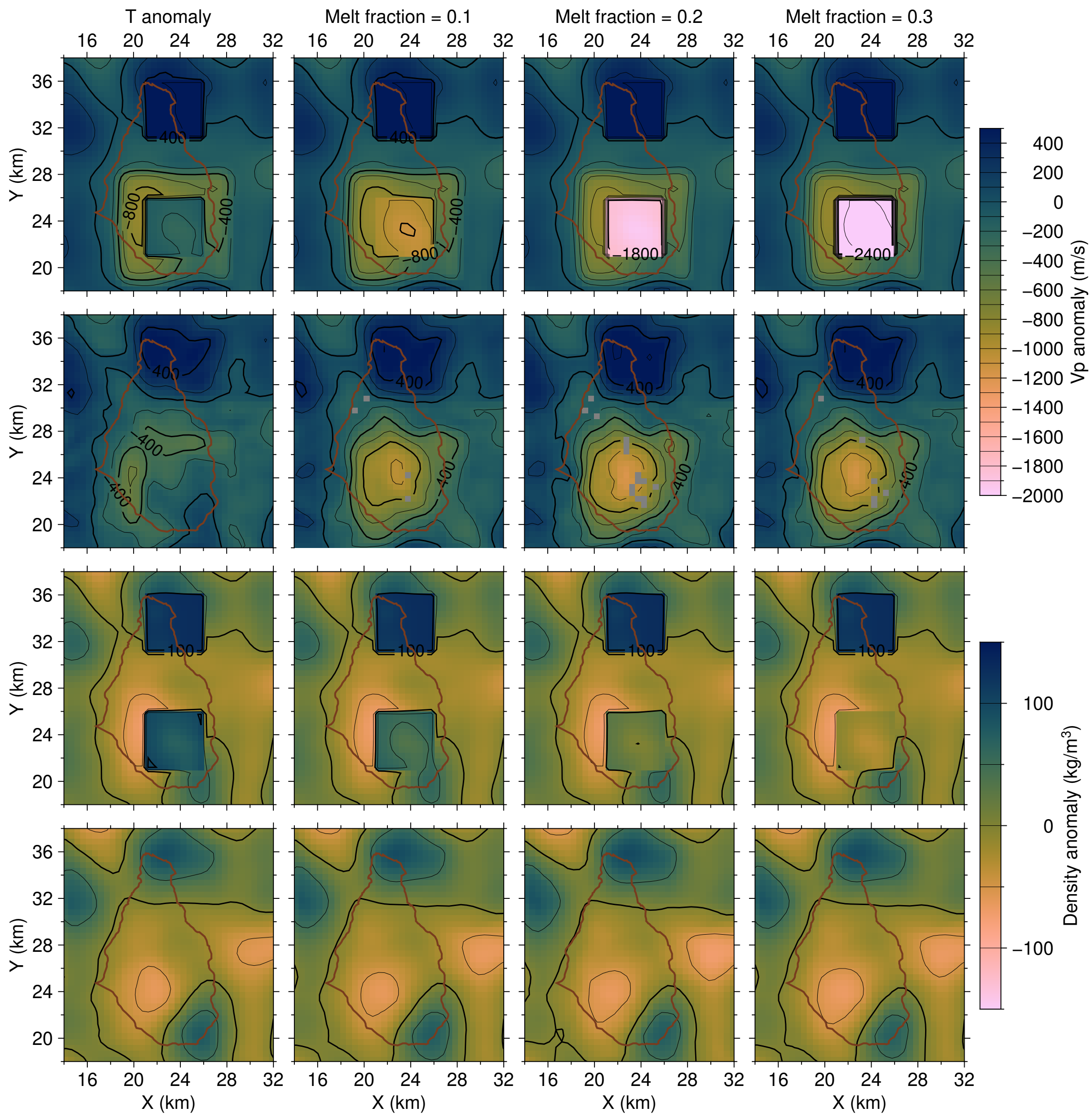

Figure S7. Anomaly recovery tests with joint inversion. We test the ability of the experiment geometry and inversion strategy to recover a series of anomalies expected for different scenarios. First column: thermal anomaly; second column: thermal anomaly plus 10% melt fraction; third column: thermal anomaly plus 20% melt fraction; fourth column: thermal anomaly plus 30% melt fraction. The density anomaly is positive since the partially molten gabbro is denser than the surrounding arc crust. Input anomalies are shown in row 1 and 3. Recovered anomalies are shown in row 2 and 4. The inversion recovers 90%, 60% and 42% of the input v_P anomaly caused by 10, 20 and 30 % melt fraction respectively and introduces some blurring and vertical smearing in the density anomaly.